Emergent Constraints on Regional Cloud Feedbacks

Nicholas Lutsko[1], Max Popp[2], Robert H. Nazarian[3], and Anna Lea Albright[4]

[1]Scripps Institution of Oceanography.
[2]Laboratoire de Météorologie Dynamique (LMD)
[3]Fairfield University
[4]LMD-IPSL

November 24, 2022

Abstract

Low-cloud based emergent constraints have the potential to substantially reduce uncertainty in Earth's Equilibrium Climate Sensitivity, but recent work has shown that previously-developed constraints fail in the latest generation of climate models, suggesting that new approaches are needed. Here, we investigate the potential for emergent constraints to reduce uncertainty in regional cloud feedbacks, rather than the global-mean cloud feedback. Strong relationships are found between the monthly/interannual variability of tropical clouds and the tropical net cloud feedback. These relationships are combined with observations to substantially narrow the uncertainty in the tropical cloud feedback and demonstrate that the tropical cloud feedback is likely > 0. Promising relationships are also found in the 90$ˆ\circ$-60$ˆ\circ$S and 30$ˆ\circ$-60$ˆ\circ$N regions, though these relationships are not robust across model generations and we have not identified the associated physical mechanisms.

Emergent Constraints on Regional Cloud Feedbacks

Nicholas J. Lutsko[1]

[1]Scripps Institution of Oceanography, University of California at San Diego, La Jolla, California.

Max Popp[2]

[2]Laboratoire de Météorologique Dynamique, Sorbonne Université, Ecole Normale Supérieure, Ecole Polytechnique, Paris, France.

Robert H. Nazarian[3]

[3]Department of Physics, Fairfield University, Fairfield, Connecticut.

Anna Lea Albright[2]

[2]Laboratoire de Météorologique Dynamique, Sorbonne Université, Ecole Normale Supérieure, Ecole Polytechnique, Paris, France.

Key Points:

- Low-cloud-based emergent constraints on Equilibrium Climate Sensitivity fail in CMIP6.
- Strong relationships are found between unforced cloud variability and long-term cloud feedbacks in several regions.
- Regional emergent constraints suggest the tropical cloud feedback is likely greater than zero.

Corresponding author: Nicholas Lutsko, `nlutsko@ucsd.edu`

Abstract

Low-cloud based emergent constraints have the potential to substantially reduce uncertainty in Earth's Equilibrium Climate Sensitivity, but recent work has shown that previously-developed constraints fail in the latest generation of climate models, suggesting that new approaches are needed. Here, we investigate the potential for emergent constraints to reduce uncertainty in regional cloud feedbacks, rather than the global-mean cloud feedback. Strong relationships are found between the monthly/interannual variability of tropical clouds and the tropical net cloud feedback. These relationships are combined with observations to substantially narrow the uncertainty in the tropical cloud feedback and demonstrate that the tropical cloud feedback is likely > 0. Promising relationships are also found in the 90°-60°S and 30°-60°N regions, though these relationships are not robust across model generations and we have not identified the associated physical mechanisms.

1 Introduction

Emergent constraints are a promising tool for constraining uncertainty in Earth's response to increased CO_2 concentrations. The power of emergent constraints lies in relating observable variables with some aspect of the climate system's forced response to substantially narrow the uncertainty in the projected climate response. The canonical example of an emergent constraint was proposed by *Hall and Qu* [2006], who demonstrated a strong correlation across climate models between the amplitude of the seasonal cycle in Northern Hemisphere snow cover and the reduction in Northern Hemisphere snow cover per degree of local warming. This strong correlation has proven to be robust across multiple climate model generations and, when combined with observations of the amplitude of Northern Hemisphere snow cover's seasonal cycle, has allowed tight constraints to be placed on the sensitivity of Northern Hemisphere snow cover to warming [*Qu and Hall*, 2014; *Thackeray et al.*, 2018].

A number of emergent constraints have been proposed for narrowing uncertainty in Earth's Equilibrium Climate Sensitivity (ECS), which can be broadly grouped into three categories: (1) constraints based on historical warming rates (e.g., *Jiménez-de-la Cuesta and Mauritsen* [2019]; *Nijsse et al.* [2020]; *Flynn and Mauritsen* [2020]), (2) constraints based on historical temperature variability (e.g., *Cox et al.* [2018]; *Nijsse et al.* [2019]), and (3) process-based constraints, often using the variability of subtropical low clouds (e.g., *Qu et al.* [2014] *Sherwood et al.* [2014]; *Brient et al.* [2016]; *Brient and Schneider* [2016]; *Siler et al.* [2018]; *Lutsko and Takahashi* [2018]). We focus here on the third type of emergent constraint. Several cloud-based emergent constraints on ECS developed using CMIP5 data proposed that constraining specific cloud processes could substantially reduce uncertainty in ECS; however, when these constraints are re-calculated using CMIP6 data the correlations between the metrics of cloud variability and models' ECS are much lower [*Schlund et al.*, 2020][1]. This puts the utility of cloud-based emergent constraints into question, and suggests that temperature-based constraints may be more fruitful approaches for constraining Earth's ECS.

One potential explanation for why cloud-based emergent constraints perform poorly in CMIP6 is that multiple factors are responsible for the spread in ECS across CMIP6 models. *Zelinka et al.* [2020] have shown that the high climate sensitivities of many CMIP6 models can be attributed in part to extratropical cloud feedbacks, including a less negative cloud feedback over the Southern Ocean, though tropical clouds still play a role. By contrast, subtropical low clouds are the main source of intermodel spread in climate feedbacks across the CMIP5 models (e.g., *Andrews et al.* [2012]; *Vial et al.* [2013]; *Sherwood et al.* [2014]; *Caldwell et al.* [2016]). If multiple cloud-types and regions are responsible for the spread in CMIP6 models' cloud feedback, then a single metric will struggle to constrain the global-mean cloud feedback, and hence will struggle to constrain ECS.

These issues suggest that emergent constraints based on cloud variability cannot be used to narrow the spread of ECS among CMIP6 models, but emergent constraints may still be of use in more limited, local contexts. For example, an emergent constraint based on subtropical low cloud variability could be used to constrain the subtropical low cloud feedback, even if it could not be used to constrain the global-mean cloud feedback. Similarly, new emergent constraints could be developed for the cloud feedback over the Southern Ocean. With this motivation, we propose here a new set of emergent constraints on regional cloud feedbacks. To develop these constraints, we have used the same metrics of cloud variability in each region: the regression of deseasonalized monthly surface temperature onto deseasonalized monthly Cloud Radiative Effect (CRE, α_m), and the regression

[1] Some cloud-based emergent constraints even perform poorly when applied to CMIP5 models not included in the original analysis [*Caldwell et al.*, 2018].

of annual-mean surface temperature onto annual-mean CRE (α_a). Using the same metrics allows us to simplify the interpretation and methodology, as new metrics do not have to be developed from scratch for each region. Instead, we can standardize the procedure for calculating the emergent constraints and using them to update the probability density functions (PDFs) of the regional cloud feedbacks. Using two predictor variables also allows us to check for consistency, as the results of emergent constraints developed with monthly variability should be consistent with the results of emergent constraints developed with interannual variability.

Taking this approach, we have investigated the links between α_m and α_a and regional cloud feedbacks in the CMIP5 and CMIP6 models. First, we demonstrate that cloud feedbacks in multiple regions contribute to the spread in CMIP6 models' ECS, whereas tropical clouds are the primary source of spread in CMIP5 model's ECS (section 3). This confirms the difficulty of constraining ECS in CMIP6 models using low-cloud based emergent constraints and motivates our regional approach. We then evaluate the relationships in each region between α_m and α_a, and the long-term regional cloud feedback (section 4). We do this for both CMIP5 and CMIP6 models to check whether viable emergent constraints are robust to the choice of models. Finally, in section 5 we use an information-theoretic approach to estimate posterior PDFs of the regional cloud feedbacks in those regions where strong correlations are found between the predictor variables and the regional cloud feedbacks. The posterior PDFs account for observational constraints on the regional cloud feedbacks, and our information-theoretic approach ensures that models that are inconsistent with observations have a small influence on the posterior PDFs.

2 Data and Methods

2.1 Observational data

To estimate the variability of regional cloudiness in observations we have taken 17 years of monthly TOA radiative fluxes, spanning the years 2003-2019, from the Clouds and the Earth's Radiant Energy System (CERES-EBAF) dataset. These are matched to surface air temperatures taken from the ERA5 dataset [*Copernicus Climate Change Service Climate Data Store (CDS)*, 2017].

2.2 CMIP data

Data are taken from 21 CMIP6 models and 22 CMIP5 models, listed in the Supplementary Material. To estimate the regional cloud feedbacks we take 500 years of data from a pre-industrial control simulation and 150 years of data from an abrupt4XCO2 simulation with each model. The data include monthly-mean values of surface air temperature, both clear-sky and all-sky TOA fluxes, and vertical pressure velocities at 500hPa (see section 4.3). To estimate α_m and α_a we use linearly de-trended data from a historical simulation with each model, and we repeat our analyses on three non-overlapping 17-year segments for each set of models (1963-1980, 1980-1997, 1997-2014 for CMIP6 and 1954-1971, 1971-1988, 1988-2005 for CMIP5), then average the results.

2.3 Estimating regional cloud feedbacks

We have calculated long-term cloud feedbacks in five regions: 90°S-60°S, 60°S-30°S, 30°S-30°N, 30°N-60°N and 60°N-90°N. In each region, we calculate the net cloud feedback using the Gregory method [*Gregory et al.*, 2004]. First, we linearly detrend the surface temperature and net (longwave plus shortwave) CRE fields, averaged over each region, from the preindustrial control simulations, then subtract these climatological values from the 4XCO2 data. The long-term regional cloud feedbacks are obtained by regressing the anomalous annual-mean surface temperature onto the anomalous annual-mean net CRE in each region for years 1-150 of the 4XCO2 simulations.

Gregory regressions are often performed for years 20-150 of 4XCO2 simulations when estimating a model's ECS, to account for the change in slope as the global-mean radiative feedback evolves [*Winton et al.*, 2010; *Geoffroy et al.*, 2013; *Andrews et al.*, 2015; *Armour*, 2017]. However, there are no clear changes of slope in the regional Gregory CRE plots (Supplemental Figure 1), and performing the regressions for years 1-150 gives similar values to performing the regressions for years 20-150, though the uncertainties are smaller when more data are used. This is consistent with the change in the net climate feedback being caused by the evolving pattern of the surface temperature response, rather than by changes in the local feedbacks [*Armour et al.*, 2013; *Andrews et al.*, 2015].

We also note that the change in regional CRE per degree of regional warming is not strictly-speaking the “cloud feedback", and does not account for cloud-masking [*Soden* *et al.*, 2004]. Nevertheless, for ease of presentation we will refer to it as the cloud feedback hereafter.

2.4 Calculating posterior PDFs of regional cloud feedbacks

The goal of the emergent constraint methodology is to update the joint multi-model prior PDF of long-term regional feedbacks P_i, based on the raw model data, using observational data to obtain a posterior joint multi-model PDF P_f. We do this following the *Brient and Schneider* [2016] procedure, with one notable difference.

The *Brient and Schneider* [2016] procedure uses an information-theoretic distance measure between the PDFs of the observed and model regression coefficients to assign a weight w_x to each model x, where $\sum_x w_x = 1$. “Good" models, which have similar regression coefficients to the observations, are weighted more heavily, and “bad" models, whose regression coefficients are far from the observations, are given less weight. In this way, the influence of bad models, which can exert a large leverage on regression slopes, is minimized.

The joint multi-model PDFs P_i and P_f are calculated using Gaussian kernel density estimates. That is, as a weighted sum of the kernel value K_x associated with each model:

$$P(C) = \sum_x w_x K_x(C), \tag{1}$$

where C is the long-term cloud feedback in a given region and

$$K_x(C) = \frac{1}{N} \sum_{z=1,N} \frac{1}{h\sqrt{2\pi}} e^{-0.5(\frac{(C_x - C_z)}{h})^2}. \tag{2}$$

N is the number of models, C_x is the regional cloud feedback for model x, C_z is the regional cloud feedback for model z and h is a bandwidth parameter, set to 0.5 in all calculations, which we found gave a good compromise between smoothing the PDFs and minimizing error. The prior PDF P_i is calculated by assigning each model an identical weight of $w_x = \frac{1}{N}$, and hence does not distinguish between good or bad models.

Calculating the posterior weights requires PDFs for α_m and α_a for each climate model and for the observational data. We assume in both models and observations that the PDFs of α_m and α_a are Gaussian, and can be characterized by their mean values and standard deviations. The mean values of α_m and α_a are given by the regression coefficients of the monthly or annual regional surface temperature onto the regional CRE. The standard deviations are estimated by multiplying the standard errors of the linear regressions by the square root of the sample sizes ($\sqrt{204}$ for the monthly data and $\sqrt{17}$ for the annual data). We note that *Brient and Schneider* [2016] used a bootstrapping procedure to estimate the standard deviations in their metric of low cloud variability, but this is difficult to use here because of the small number of samples for the annual-mean data.

Together with the mean values of the regression slopes, the standard deviations are used to generate Gaussian PDFs of α_m and α_a for each model and for the observations. The model PDFs are denoted by $M_{m,x}$ and $M_{a,x}$ for the monthly and annual variability, respectively, and the observational PDFs are denoted by O_m and O_a. Note that we calculate three sets of model PDFs, one for each 17-year interval.

Next, we calculate the Kullback-Leibler divergence for each model PDF:

$$\Delta_x = \int O(\alpha) \log\left(\frac{O(\alpha)}{M_x(\alpha)}\right) d\alpha, \tag{3}$$

where we have dropped the m and a subscripts for convenience, but note that two sets of Δ_x values are calculated for each 17-year period. Δ_x is the relative entropy between O and M_x, and measures how much information is lost if M_x is used to approximate O. Importantly, this assumes the time-series used to estimate M_x is the same length as the time-series used to estimate O. The likelihood of model x giving rise to the observed distribution O is the exponential $l_x = \exp(-\Delta_x)$, so that normalized weights can be calculated as $w_x = \frac{l_x}{\sum_x l_x}$. Similar to weights in Bayesian model averages, the values of w_x can be interpreted as the posterior probability that model x is the best model for the data according to the Kullback–Leibler measure [*Brient and Schneider*, 2016].

3 Sources of Intermodel Spread in ECS

The regional cloud feedbacks, calculated as described in section 2.3, can be used to quantify the contributions different regions make to the intermodel spread in ECS. For example, the top row of Figure 1 demonstrates that in CMIP5 the tropical cloud feedback is highly correlated with ECS ($r^2 = 0.54$, all ECS values are taken from *Zelinka et al.* [2020]), while the cloud feedbacks in all other regions are not well correlated with ECS. Hence the tropical cloud feedback is the main source of uncertainty in CMIP5 models' ECS.

By contrast, in CMIP6 the cloud feedbacks in multiple regions are well correlated with ECS (bottom row of Figure 1; we define a correlation as statistically significant if its

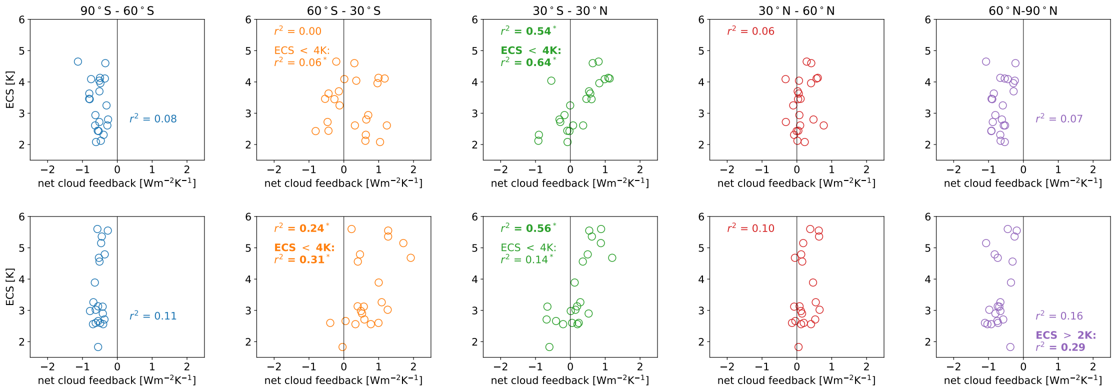

Figure 1. ECS values of the 22 CMIP5 (top) and 21 CMIP6 (bottom) models, plotted versus the regional cloud feedbacks in the five regions. r^2 values for correlations between ECS and the regional cloud feedbacks are written in each panel, with bold values and asterisks denoting correlations with p-values less than 0.05, which we take as a measure of statistical significance. The panels for 60°-30°S and 30°S-30°N also show r^2 values for correlations over models with ECS<4K, and the 60°-90°N panels show r^2 values for correlations over models with ECS>2K.

associated p-value is less than 0.05). The correlation between the tropical cloud feedback and ECS again has a high r^2 value of 0.56, but the correlation between the cloud feedback in the Southern Hemisphere mid-latitudes and ECS is also statistically significant (r^2 = 0.24). Interestingly, the Arctic cloud feedback shows a strong relationship with ECS when an outlier model (INM-CM4-8) which has an ECS of less than 2K, is ignored (r^2 = 0.29).

To investigate these relationships further, we have divided the CMIP6 models into high sensitivity (ECS > 4K) and low sensitivity (ECS < 4K) models. Repeating the correlations, we find that the tropical cloud feedback is not well correlated with the low sensitivity models' ECS (r^2 = 0.14, Figure 1), while the correlation with the Southern Hemisphere mid-latitude cloud feedback is stronger for the low sensitivity models (r^2 = 0.31; the tropical and Southern Hemisphere mid-latitude clouds feedbacks are poorly correlated among the low ECS models). Thus in CMIP6, tropical cloud feedbacks can distinguish very high climate sensitivity models from lower sensitivity models, but cannot distinguish between a 2K and a 4K model. Conversely, the Southern Hemisphere mid-latitudes can distinguish between 2K and 4K models, but are less useful for evaluating high climate sensitivities.

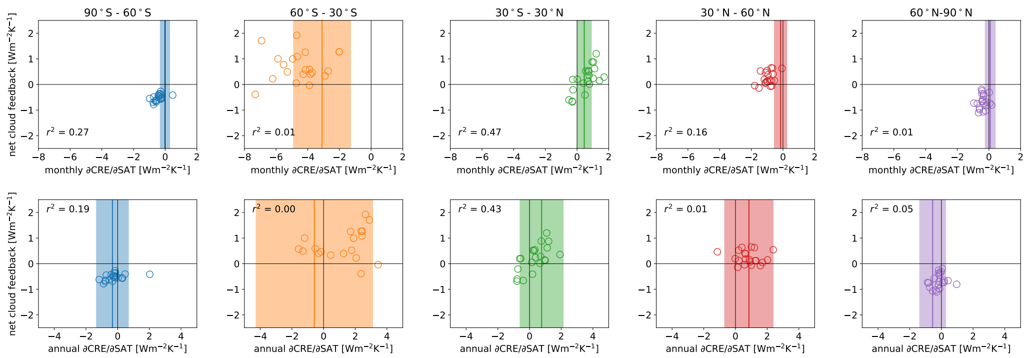

Figure 2. Mean values of α_m (top row) and α_a (bottom row) in the five geographic regions plotted versus the net cloud feedback in each region for 21 CMIP6 models. Only the regression coefficients calculated using the last 17 years of each historical simulation are shown. The shaded regions show 5-95% confidence intervals for estimates of the linear regressions from CERES-EBAF data, with the solid lines showing the mean of the observational regression estimates.

These results demonstrate why low-cloud based emergent constraints perform poorly in CMIP6: a model with a large positive tropical cloud feedback likely has a high ECS, but a model with a negative tropical cloud feedback, or a tropical cloud feedback close to zero, could have an ECS of 2K or 4K. In contrast, dividing the CMIP5 models into high and low sensitivity models still gives robust relationships between tropical clouds and ECS (Figure 1).

4 Evaluating Regional Emergent Constraints

4.1 Robust relationships

There are several robust relationships between the metrics of variability α_m and α_a and the regional cloud feedbacks. Most notably, the regression coefficients for both monthly and interannual variability in the tropics (30°S to 30°N) are highly correlated with the tropical cloud feedback in both sets of models (Table 1, Figure 2, Supplemental Figure S2). Other notable relationships are seen for the 90°-60°S region in CMIP6, and the 30°-60°N region in CMIP5. In both cases, two out of the three correlations are statistically significant, while the p-value for the third correlation is just over the 0.05 threshold.

Table 1. r^2 values for correlations across the models between α_m/α_a in each region and the long term regional cloud feedbacks. Columns 2 and 3 show three sets of values, one for each 17-year period of the historical simulations. Columns 4 and 5 show correlations when α_m and α_a are estimated using the last 50 years of each simulation. Correlations with a p-value less than 0.05, which we use as a measure of statistical significance, are in bold.

Region	17-year α_m	17-year α_a	50-year α_m	50-year α_a
CMIP6				
90°S-60°S	**0.25**/0.19/**0.27**	0.12/0.10/0.19	**0.23**	**0.19**
60°S-30°S	0.08/0.08/0.01	0.08/0.08/0.00	**0.31**	**0.34**
30°S-30°N	**0.37/0.60/0.47**	**0.28/0.50/0.43**	**0.44**	**0.59**
30°N-60°N	0.11/0.11/0.16	0.04/**0.21**/0.01	**0.20**	0.08
60°N-90°N	0.05/0.07/0.01	0.03/0.10/0.05	0.0	0.02
CMIP5				
90°S-60°S	0.0/0.0/0.0	0.18/0.02/0.07	0.08	0.09
60°S-30°S	0.0/0.0/0.01	0.03/0.18/**0.29**	0.09	**0.33**
30°S-30°N	**0.47/0.35/0.51**	**0.59/0.42/0.36**	**0.60**	**0.60**
30°N-60°N	0.15/**0.27/0.26**	0.03/**0.28**/0.17	**0.35**	**0.26**
60°N-90°N	0.02/0.0/0.0	0.04/0.08/0.0	0.03	0.01
Joint				
90°S-60°S	0.03/0.01/0.02	0.09/0.03/0.09	**0.11**	0.08
60°S-30°S	0.01/0.00/0.00	0.13/0.01/**0.13**	**0.13**	**0.38**
30°S-30°N	**0.41/0.39/0.42**	**0.46/0.42/0.38**	**0.49**	**0.59**
30°N-60°N	**0.15/0.23/0.23**	0.00/**0.21**/0.06	**0.28**	**0.19**
60°N-90°N	0.01/0.03/0.00	0.02/0.1/0.00	0.02	0.03

The observed α_m values for the 30°-60°N region are outside the intermodel spread in CMIP5 (Supplemental Figure 2), implying that all models struggle to simulate cloud variability in this region and that we should be cautious about using this relationship to update the regional cloud feedback. Nevertheless, the observations and implied relationship do suggest that the regional cloud feedback in this region is more positive than is simulated by the models. For the 90°-60°S region, there is one outlier model (CNRM-CM6-1) which is far from the observations and from the other models. Disregarding this model increases the correlation between α_m and the regional cloud feedback slightly (not shown), but our methodology will anyways assign a small weight to this model when calculating the posterior PDF.

As another test of the robustness of these relationships, we have taken correlations across the joint ensemble of CMIP5 and CMIP6 data. The r^2 values of these correlations are consistent with the findings from the individual ensembles (third set of rows in Table 1), with the exception of the 90°-60°S region, for which the high correlations found in CMIP6 disappear in the joint ensemble. This is not surprising, since the correlations in this region are very low in CMIP5, but suggest further caution.

4.2 Using longer time-series

17 years of observational data is a short record with which to search for robust correlations, but the methodology used to calculate the posterior PDFs requires that the model and observational time-series have the same lengths. To investigate whether more robust relationships emerge with longer datasets, we have also calculated the variability coefficients α_m and α_a using the last 50 years of the historical simulations (1964 – 2014 in CMIP6 and 1955 – 2005 in CMIP5). Correlating these new coefficients with the regional cloud feedbacks gives stronger relationships than the 17 year coefficients (Table 1, Supplemental Figures S3 and S4), with statistically significant relationships between α_m and/or α_a and the cloud feedbacks in all regions except for the high northern latitudes (60°-90°N).

The strong correlations for the 60°S-30°S region[2] are of particular interest, as the Southern Hemisphere mid-latitudes have been identified as one of the causes of the high

[2] The low correlation for the CMIP5 α_ms is due to an outlier model. See Supplemental Figure S4.

climate sensitivities in certain CMIP6 models [*Zelinka et al.*, 2020]. The calculations in section 3 further demonstrate the importance of this region for the spread in ECS among CMIP6 models. However, our previous calculations demonstrated that the relationships between monthly/interannual variability of surface temperature and CRE in the Southern Hemisphere mid-latitudes cannot be robustly identified from 17 years of observational data, so we cannot use observations and the methodology described in section 2.4 to constrain the cloud feedback in this region. Moreover, the large observational uncertainty in this region suggests that emergent relationships are unlikely to be of practical use for constraining the 60°S-30°S cloud feedback in the near future, even with other methodologies.

4.3 Explaining the high correlations in the tropics

Emergent constraints are sometimes criticised as being the result of data mining (*Caldwell et al.* [2014, 2018]; *Hall et al.* [2019]), with no physical basis for the proposed relationships. Here, our starting assumption is that the intermodel spread in cloud physics is time-scale invariant (note that we are not assuming the cloud physics itself is invariant, but that the causes of intermodel spread are invariant). This is reasonable in the tropics, where previous emergent constraints have linked the variability of specific tropical and subtropical clouds to the net cloud feedback (e.g., *Zhai et al.* [2015]; *Brient and Schneider* [2016]; *Lutsko* [2018]). Moreover, our results demonstrate that the unforced variability of the tropical-mean cloud feedback, which includes contributions from all tropical cloud-types, is related to the forced tropical-mean cloud feedback. This suggests that the same clouds are responsible for intermodel spread in the variability and in the cloud feedback. To confirm this, we have binned the net CRE and surface temperature values based on the corresponding pressure velocities at 500hPa (ω_{500}), which is an effective method for separating out different cloud regimes in the tropics, where high clouds tend to form in regions of large-scale ascent and low clouds tend to form in regions of large-scale descent [*Bony et al.*, 2004; *Bony and Dufresne*, 2005]. The left panels of Figure 3 show the tropical cloud feedback in each ω_{500} bin, and the right panels show correlations between the monthly/annual variability of tropical net CRE in each ω_{500} bin and the monthly/annual variability of tropical-mean net CRE over the historical simulations. Clouds in regimes of weak-to-moderate descent clearly make the largest contributions to the tropical cloud feedback (left panels) and also have the highest correlations with the tropical-mean CRE (right panels), consistent with the large statistical weight of these subtropical low clouds

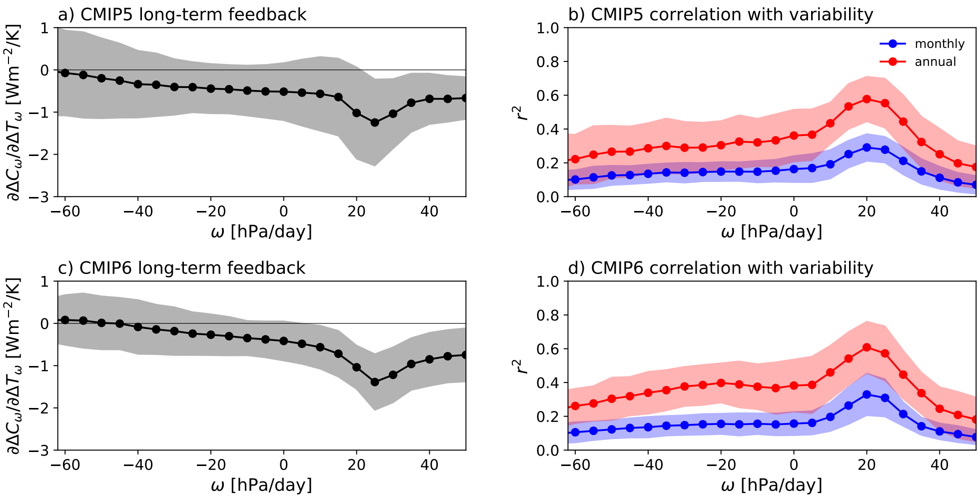

Figure 3. a) Long-term CMIP5 tropical cloud feedback in ω_{500} bins, calculated following *Bony and Dufresne* [2005] by dividing the long-term tropical net CRE trend in each 5hPa bin over years 1-150 of abrupt4XCO2 simulations by the long-term surface temperature trend in each bin. The black markers show the multi-model mean values and the gray shading shows ±1 standard deviation. b) r^2 values for correlations in the CMIP5 models between the monthly (blue) and annual-mean (red) CRE in each 5hPa bin and the tropical-mean CRE over the final 50 years of the historical simulations. The markers show the multi-model mean values and the shadings show ±1 standard deviation. c) Same as panel a but for CMIP6 models. d) Same as panel b but for CMIP6 models.

[*Bony and Dufresne*, 2005]. Hence in both sets of models, our simple metrics of tropical cloud variability mostly reflect the contributions of low clouds to monthly and interannual cloud variability, and these clouds are also the main source of uncertainty in the long-term tropical cloud feedback.

These results are consistent with *Lutsko* [2018], who showed that (in models) the variations in tropical CRE during the ENSO cycle are mostly due to low clouds, with high and mid-level clouds making minor contributions. So, while high and mid-level clouds may show substantial differences in spatial organization on monthly, annual and ENSO time-scales, they make relatively small contributions to the variability of the tropical-mean radiation budget.

The physical mechanisms linking variability in other regions and the regional cloud feedbacks are less clear, and may be more difficult to identify, given the larger seasonal

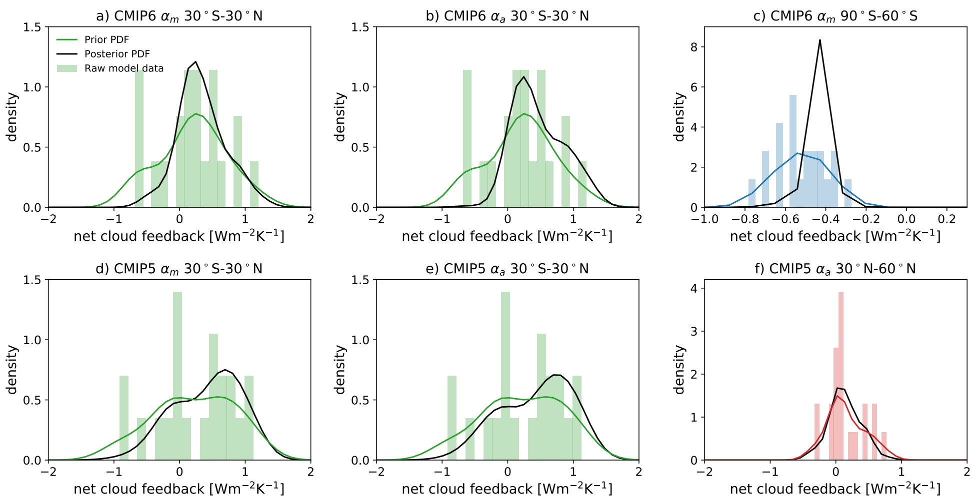

Figure 4. a) Prior and posterior PDFs of the tropical cloud feedback in CMIP6. The green bars show the raw model distribution of tropical cloud feedbacks and the green curves show the prior PDFs estimated using Gaussian kernel estimates. The black curves show the posterior PDFs obtained using monthly variability, following the procedure described in section 2.4. b) Same as panel a but the posterior PDF is obtained using interannual variability. c) Prior and posterior PDFs of the cloud feedback in the 90°-60°S region in CMIP6. The blue bars show the raw model distribution of regional cloud feedbacks and the blue curves show the prior PDFs estimated using Gaussian kernel estimates. The black curves show the posterior PDFs obtained using monthly variability, following the procedure described in section 2.4. d) Same as panel a but for the CMIP5 models. e) Same as panel b but for CMIP5 data. f) Prior and posterior PDFs of the cloud feedback in the 30°-60°N region in CMIP5. The red bars show the raw model distribution of regional cloud feedbacks and the red curves show the prior PDFs estimated using Gaussian kernel estimates. The black curves show the posterior PDFs obtained using monthly variability, following the procedure described in section 2.4.

cycles at higher latitudes. We leave it to future work to identify the mechanisms, but note again that the results for 90°-60°S and 30°-60°N should be taken with caution until physical mechanisms can be identified.

5 Constraining Regional Cloud Feedbacks

Section 4 established the existence of robust relationships between the variability of tropical cloudiness on monthly and interannual time-scales, and the long-term tropical cloud feedback. Statistically significant relationships were also found in the CMIP6 models between the monthly variability of cloudiness and the regional cloud feedback at 90°-60°S and in CMIP5 between the monthly variability of cloudiness and the regional cloud feedback at 30°-60°N, though these relationships are less robust, particularly since they are only found in one generation of models. Using the procedure described in section 2.4, we have estimated posterior PDFs for the cloud feedbacks in the three regions, with the results shown in Figure 4 (the posterior weights are listed in Supplemental Tables S1 and S2).

In both sets of models, the monthly and interannual results for the tropics are remarkably similar. Panels a and d show that using α_m and α_a with the CMIP6 data results in very similar posterior tropical cloud feedback PDFs, while panels b and e show the same for the CMIP5 data. In both sets of models, and for both α_m and α_a, the posterior PDFs are weighted more heavily towards positive values than the prior PDFs. This is particularly true in the CMIP6 models, where the posterior PDF is considerably narrower: in CMIP6 the 5-95 percentile confidence intervals go from -0.65 - 1.26 Wm^{-2} / K in the prior PDF to 0.06 - 1.37 Wm^{-2} / K in the posterior PDF obtained using annual data or -0.09 - 1.18 Wm^{-2} / K in the posterior PDF obtained using monthly data. In CMIP5 the 5-95 percentile confidence intervals go from -0.77 - 1.38 Wm^{-2} / K in the prior PDF to -0.39 - 1.44 Wm^{-2} / K in the posterior PDF obtained using annual data or -0.32 - 1.40 Wm^{-2} / K in the posterior PDF obtained using monthly data. The shifts of the posterior PDFs towards more positive values are consistent with other lines of evidence pointing to a positive tropical cloud feedback [*Myers and Norris*, 2016; *Klein et al.*, 2018; *Scott et al.*, 2020; *Sherwood et al.*, 2020]. We have not investigated why the posterior PDFs are narrower when using the CMIP6 data than when using the CMIP5 data, but note that the distribution of tropical cloud feedbacks in CMIP5 is more bimodal than in CMIP6, with maxima close to 0Wm^{-2}/K and near 0.8Wm^{-2}/K. The posterior PDFs retain this bimodality, but with more weight on the maximum at 0.8Wm^{-2}/K.

For the other two regions, the posterior PDF for 90°S-60°S has a strong peak at around -0.5Wm^{-2}/K and is substantially narrower than the prior; while the posterior PDF for 30°-60°N is only slightly narrower than the prior. Thus an emergent constraint based on the monthly variability at 90°S-60°S has the potential to strongly constrain the cloud feedback in this region, though more work is needed to confirm this result. It will be difficult to use emergent constraints for the feedback at 30°-60°N since the models do a poor job at reproducing the variability in this region.

6 Conclusion

The results presented here demonstrate that both the monthly and the interannual variability of cloudiness in the tropics can be used to constrain the tropical cloud feedback, with CMIP5 and CMIP6 results suggesting that the tropical cloud feedback is on the higher end of the intermodel range, and likely greater than zero. This is consistent with recent work using cloud-controlling factors to constrain the tropical cloud feedback [*Myers and Norris*, 2016; *Klein et al.*, 2018; *Scott et al.*, 2020]. At higher latitudes, we have tentatively shown that emergent constraints can be applied to the regional cloud feedbacks at 90°-60°S and 30°-60°N; with the variability in the 90°-60°S region showing particular promise as the basis for an emergent constraint. However, the high correlations between the monthly variability and cloud feedbacks in these regions are not robust across both generations of models, and we have not identified the physical mechanisms responsible for the relationships.

Another factor which limits the effectiveness of cloud-based emergent constraints is the relatively short length of the satellite record (~17 years). Using 50 years of model data, we have found statistically significant relationships between cloud variability and regional cloud feedbacks in all regions except for 60°-90°N. This hints that the cloud feedback in the Southern Hemisphere mid-latitudes (60°-30°S), a key region for the high climate sensitivities of CMIP6 models, could be constrained using the local unforced variability. Unfortunately, our metrics of variability have the highest observational uncertainty in this region, and more data will be needed before emergent constraints can be used to constrain the cloud feedback in the Southern Hemisphere mid-latitudes. Other approaches, for example which focus on the simulation of specific cloud properties (e.g., *Ceppi et al.* [2016]), may be more successful moving forward.

Cloud-based emergent constraints developed in CMIP5 consistently indicated ECS is on the higher end of the intermodel range (3-4°C, see *Bretherton and Caldwell* [2020]), in contrast to recent temperature-based emergent constraints which generally indicate lower ECS values (2-3°C, e.g., *Cox et al.* [2018]; *Jiménez-de-la Cuesta and Mauritsen* [2019]). Reconciling these two opposing lines of evidence is of crucial importance for improving our confidence in ECS estimates. While the failure of cloud-based emergent constraints in CMIP6 does not rule out the possibility of high ECS values, it does suggest that a more nuanced approach, moving cloud-type by cloud-type and region-by-region, will be required to reduce uncertainty in Earth's cloud feedback.

Acknowledgments

We thank Joel Norris for helpful discussions and comments on an earlier version of this manuscript. N.J.L. was supported by the NOAA Climate Program Office's Modeling, Analysis, Predictions, and Projections program through grant NA20OAR4310387. M. P. acknowledges funding from the Centre National D' études Spatiales (CNES). The CMIP5 and CMIP6 data are publicly available at: https://esgf-node.llnl.gov/projects/esgf-llnl/, the ERA5 data are publicly available at: https://www.ecmwf.int/en/forecasts/datasets/reanalysis-datasets/era5 and the CERES-EBAF data are publicly available from: https://ceres.larc.nasa.gov/data/. Jupyter notebooks with the analysis and processing scripts are available at *Lutsko* [2021].

References

Andrews, T., J. M. Gregory, M. J. Webb, and K. E. Taylor (2012), Forcing, feedbacks and climate sensitivity in cmip5 coupled atmosphere-ocean climate models, *Geophysical Research Letters*, *39*(9), l09712.

Andrews, T., J. M. Gregory, and M. J. Webb (2015), The dependence of radiative forcing and feedback on evolving patterns of surface temperature change in climate models., *Journal of Climate*, *28*(2), 1630–1648.

Armour, K. C. (2017), Energy budget constraints on climate sensitivity in light of inconstant climate feedbacks, *Nature Climate Change*, *7*(5), 331–335, doi: 10.1038/nclimate3278, number: 5 Publisher: Nature Publishing Group.

Armour, K. C., C. M. Bitz, and G. H. Roe (2013), Time-Varying Climate Sensitivity from Regional Feedbacks, *Journal of Climate*, *26*(13), 4518–4534, doi:10.1175/JCLI-D-12-00544.1.

Bony, S., and J. L. Dufresne (2005), Marine boundary layer clouds at the heart of tropical cloud feedback uncertainties in climate models., *Geophysical Research Letters*, *32*(6), L20,806.

Bony, S., J.-L. Dufresne, H. Le Treut, J.-J. Morcrette, and C. Senior (2004), On dynamic and thermodynamic components of cloud changes, *Climate Dynamics*, *22*(2), 71–86, doi:10.1007/s00382-003-0369-6.

Bretherton, C. S., and P. M. Caldwell (2020), Combining Emergent Constraints for Climate Sensitivity, *Journal of Climate*, *33*(17), 7413–7430, doi:10.1175/JCLI-D-19-0911.1, publisher: American Meteorological Society Section: Journal of Climate.

Brient, F., and T. Schneider (2016), Constraints on Climate Sensitivity from Space-Based Measurements of Low-Cloud Reflection, *Journal of Climate*, *29*(16), 5821–5835.

Brient, F., T. Schneider, Z. Tan, S. Bony, X. Qu, and A. Hall (2016), Shallowness of tropical low clouds as a predictor of climate models' response to warming, *Climate Dynamics*, *47*(1-2), 433–449.

Caldwell, P. M., C. S. Bretherton, M. D. Zelinka, S. A. Klein, B. D. Santer, and B. M. Sanderson (2014), Statistical significance of climate sensitivity predictors obtained by data mining, *Geophysical Research Letters*, *41*(5), 1803–1808, doi:https://doi.org/10.1002/2014GL059205, _eprint: https://agupubs.onlinelibrary.wiley.com/doi/pdf/10.1002/2014GL059205.

Caldwell, P. M., M. D. Zelinka, K. E. Taylor, and K. Marvel (2016), Quantifying the Sources of Intermodel Spread in Equilibrium Climate Sensitivity, *Journal of Climate*, *29*(2), 513–524, doi:10.1175/JCLI-D-15-0352.1, publisher: American Meteorological Society Section: Journal of Climate.

Caldwell, P. M., M. D. Zelinka, and S. A. Klein (2018), Evaluating Emergent Constraints on Equilibrium Climate Sensitivity, *Journal of Climate*, *31*(10), 3921–3942, doi:10.1175/JCLI-D-17-0631.1, publisher: American Meteorological Society Section: Journal of Climate.

Ceppi, P., D. T. McCoy, and D. L. Hartmann (2016), Observational evidence for a negative shortwave cloud feedback in middle to high latitudes, *Geophysical Research Letters*, *43*(3), 1331–1339, doi:10.1002/2015GL067499.

Copernicus Climate Change Service Climate Data Store (CDS) (2017), Copernicus Climate Change Service (c3s) (2017): ERA5: Fifth generation of ECMWF atmospheric reanalyses of the global climate, accessed 02 March 2018, https://cds.climate.copernicus.eu/cdsapp!/home.

Cox, P. M., C. Huntingford, and M. S. Williamson (2018), Emergent constraint on equilibrium climate sensitivity from global temperature variability, *Nature*, *553*(7688), 319–322, doi:10.1038/nature25450, number: 7688 Publisher: Nature Publishing Group.

Flynn, C. M., and T. Mauritsen (2020), On the climate sensitivity and historical warming evolution in recent coupled model ensembles, *Atmospheric Chemistry and Physics*, *20*(13), 7829–7842, doi:10.5194/acp-20-7829-2020.

Geoffroy, O., D. Saint-Martin, G. Bellon, A. Voldoire, D. J. L. Olivie, and S. Tyteca (2013), Transient climate response in a two-layer energy-balance model. part ii: Representation of the efficacy of deep-ocean heat uptake and validation for cmip5 aogcms, *Journal of Climate*, *26*(6), 1859–1876.

Gregory, J. M., W. J. Ingram, M. A. Palmer, G. S. Jones, P. A. Stott, R. B. Thorpe, J. A. Lowe, T. C. Johns, and K. D. Williams (2004), A new method for diagnosing radiative forcing and climate sensitivity, *Geophysical Research Letters*, *31*, L03,205.

Hall, A., and X. Qu (2006), Using the current seasonal cycle to constrain snow albedo feedback in future climate change., *Geophysical Research Letters*, *33*(23), 2006GL03502.

Hall, A., P. Cox, C. Huntingford, and S. Klein (2019), Progressing emergent constraints on future climate change, *Nature Climate Change*, *9*(4), 269–278, doi:10.1038/s41558-019-0436-6, number: 4 Publisher: Nature Publishing Group.

Jiménez-de-la Cuesta, D., and T. Mauritsen (2019), Emergent constraints on Earth's transient and equilibrium response to doubled CO 2 from post-1970s global warming, *Nature Geoscience*, *12*(11), 902–905, doi:10.1038/s41561-019-0463-y, number: 11 Publisher: Nature Publishing Group.

Klein, S. A., A. Hall, J. R. Norris, and R. Pincus (2018), Low-Cloud Feedbacks from Cloud-Controlling Factors: A Review, in *Shallow Clouds, Water Vapor, Circulation, and Climate Sensitivity*, edited by R. Pincus, D. Winker, S. Bony, and B. Stevens, pp. 135–157, Springer International Publishing, Cham, doi:10.1007/978-3-319-77273-8$_7$.

Lutsko, N. J. (2018), The relationship between cloud radiative effect and surface temperature variability at enso frequencies in cmip5 models., *Geophysical Research Letters*, *45*, 10,599 – 10,608.

Lutsko, N. J. (2021), nicklutsko/regional$_emergent_constraints$: $Firstrelease(versionv1.0.0).,doi:http://doi.org/10.5281/zenodo.4531393$.

Lutsko, N. J., and K. Takahashi (2018), What can the internal variability of cmip5 models tell us about their climate sensitivity?, *Journal of Climate*, *31*, 5051 – 5069.

Myers, T. A., and J. R. Norris (2016), Reducing the uncertainty in subtropical cloud feedback, *Geophysical Research Letters*, *43*(5), 2144–2148, doi:https://doi.org/10.1002/2015GL067416, _eprint: https://agupubs.onlinelibrary.wiley.com/doi/pdf/10.1002/2015GL067416.

Nijsse, F. J. M. M., P. M. Cox, C. Huntingford, and M. S. Williamson (2019), Decadal global temperature variability increases strongly with climate sensitivity, *Nature Climate Change*, *9*(8), 598–601, doi:10.1038/s41558-019-0527-4, number: 8 Publisher: Nature Publishing Group.

Nijsse, F. J. M. M., P. M. Cox, and M. S. Williamson (2020), Emergent constraints on transient climate response (TCR) and equilibrium climate sensitivity (ECS) from historical warming in CMIP5 and CMIP6 models, *Earth System Dynamics*, *11*(3), 737–750, doi: 10.5194/esd-11-737-2020.

Qu, X., and A. Hall (2014), On the persistent spread in snow-albedo feedback, *Climate Dynamics*, *42*(1), 69–81, doi:10.1007/s00382-013-1774-0.

Qu, X., A. Hall, S. A. Klein, and P. M. Caldwell (2014), On the spread of changes in marine low cloud cover in climate model simulations of the 21st century, *Climate Dynamics*, *42*(9), 2603–2626, doi:10.1007/s00382-013-1945-z.

Schlund, M., A. Lauer, P. Gentine, S. C. Sherwood, and V. Eyring (2020), Emergent constraints on equilibrium climate sensitivity in CMIP5: do they hold for CMIP6?, *Earth System Dynamics*, *11*(4), 1233–1258, doi:10.5194/esd-11-1233-2020.

Scott, R. C., T. A. Myers, J. R. Norris, M. D. Zelinka, S. A. Klein, M. Sun, and D. R. Doelling (2020), Observed Sensitivity of Low-Cloud Radiative Effects to Meteorological Perturbations over the Global Oceans, *Journal of Climate*, *33*(18), 7717–7734, doi: 10.1175/JCLI-D-19-1028.1, publisher: American Meteorological Society Section: Journal of Climate.

Sherwood, S. C., S. Bony, and J.-L. Dufresne (2014), Spread in model climate sensitivity traced to atmospheric convective mixing, *Nature*, *505*, 37–42.

Sherwood, S. C., M. J. Webb, J. D. Annan, K. C. Armour, P. M. Forster, J. C. Hargreaves, G. Hegerl, S. A. Klein, K. D. Marvel, E. J. Rohling, M. Watanabe, T. Andrews, P. Braconnot, C. S. Bretherton, G. L. Foster, Z. Hausfather, A. S. v. d. Heydt, R. Knutti, T. Mauritsen, J. R. Norris, C. Proistosescu, M. Rugenstein, G. A. Schmidt, K. B. Tokarska, and M. D. Zelinka (2020), An assessment of Earth's climate sensitivity using multiple lines of evidence, *Reviews of Geophysics*, *n/a*(n/a), e2019RG000,678.

Siler, N., S. Po-Chedley, and C. S. Bretherton (2018), Variability in modeled cloud feedback tied to differences in the climatological spatial pattern of clouds, *Climate Dynamics*, *50*(3), 1209–1220, doi:10.1007/s00382-017-3673-2.

Soden, B. J., A. J. Broccoli, and R. S. Hemler (2004), On the Use of Cloud Forcing to Estimate Cloud Feedback, *Journal of Climate*, *17*(19), 3661–3665, doi:10.1175/1520-0442(2004)017<3661:OTUOCF>2.0.CO;2, publisher: American Meteorological Society Section: Journal of Climate.

Thackeray, C. W., X. Qu, and A. Hall (2018), Why Do Models Produce Spread in Snow Albedo Feedback?, *Geophysical Research Letters*, *45*(12), 6223–6231, doi:https://doi.org/10.1029/2018GL078493, _eprint: https://agupubs.onlinelibrary.wiley.com/doi/pdf/10.1029/2018GL078493.

Vial, J., J.-L. Dufresne, and S. Bony (2013), On the interpretation of inter-model spread in cmip5 climate sensitivity estimates., *Climate Dynamics*, *41*(1), 3339–3362.

Winton, M., K. Takahashi, and I. M. Held (2010), Importance of ocean heat uptake efficacy to transient climate change, *Journal of Climate*, *23*(6), 2333–2344.

Zelinka, M. D., T. A. Myers, D. T. McCoy, S. Po-Chedley, P. M. Caldwell, P. Ceppi, S. A. Klein, and K. E. Taylor (2020), Causes of Higher Climate Sensitivity in CMIP6 Models, *Geophysical Research Letters*, *47*(1), e2019GL085,782.

Zhai, C., J. H. Jiang, and H. Su (2015), Long-term cloud change imprinted in seasonal cloud variation: More evidence of high climate sensitivity, *Geophysical Research Letters*, *42*(20), 8729–8737, doi:https://doi.org/10.1002/2015GL065911, _eprint: https://agupubs.onlinelibrary.wiley.com/doi/pdf/10.1002/2015GL065911.

Figure 1.

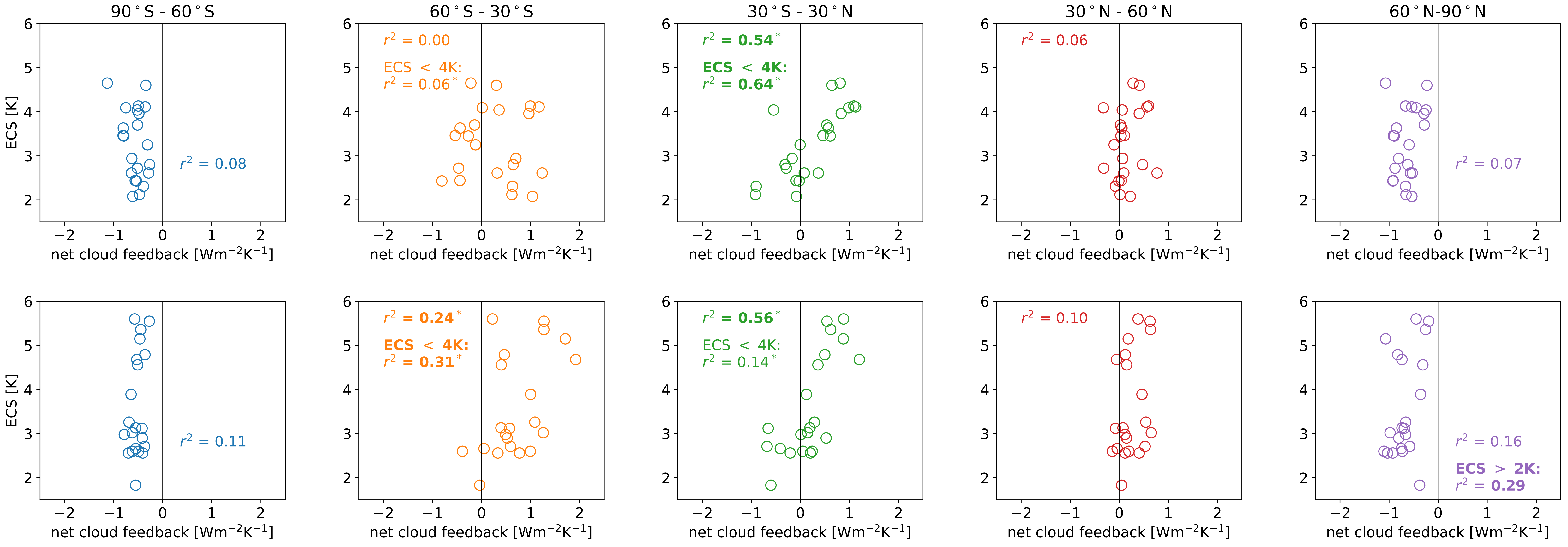

90°S - 60°S
60°S - 30°S
30°S - 30°N
30°N - 60°N
60°N-90°N
ECS [K]
net cloud feedback [Wm^{-2}K^{-1}]
r^2 = 0.08
r^2 = 0.00
ECS < 4K:
r^2 = 0.06*
r^2 = 0.54*
ECS < 4K:
r^2 = 0.64*
r^2 = 0.06
r^2 = 0.07
r^2 = 0.11
r^2 = 0.24*
ECS < 4K:
r^2 = 0.31*
r^2 = 0.56*
ECS < 4K:
r^2 = 0.14*
r^2 = 0.10
r^2 = 0.16
ECS > 2K:
r^2 = 0.29

Figure 2.

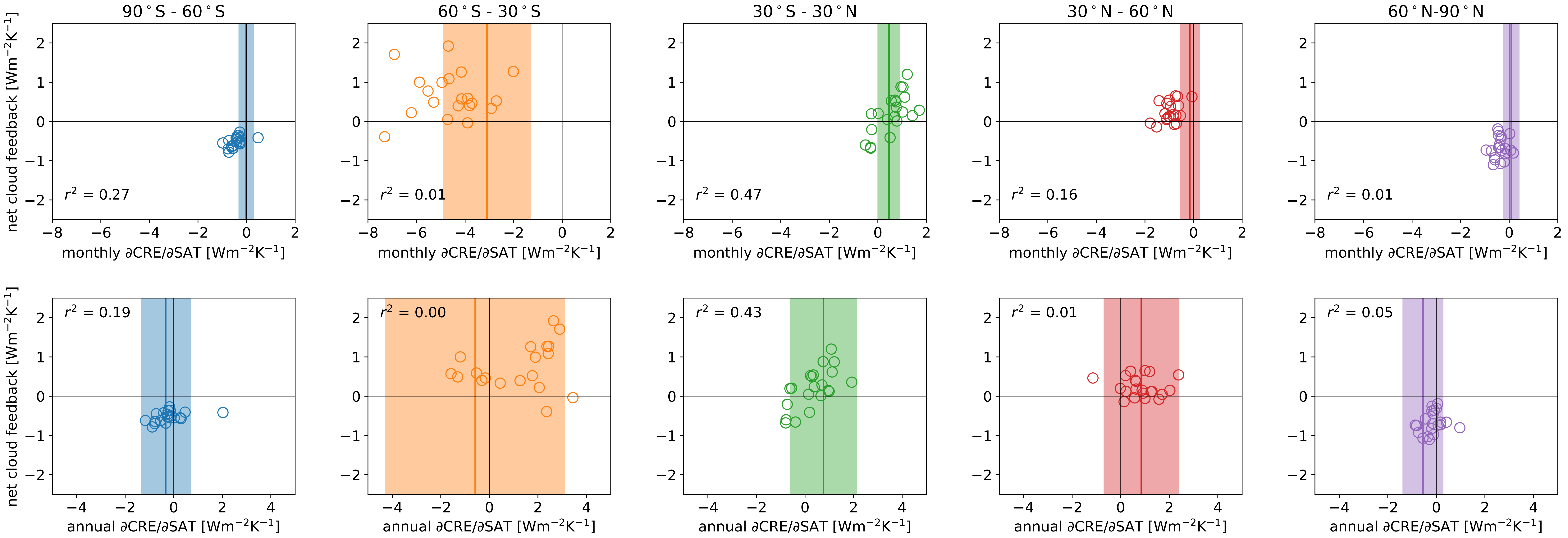
90°S - 60°S
60°S - 30°S
30°S - 30°N
30°N - 60°N
60°N-90°N
net cloud feedback [Wm^{-2}K^{-1}]
monthly ∂CRE/∂SAT [Wm^{-2}K^{-1}]
annual ∂CRE/∂SAT [Wm^{-2}K^{-1}]
r^2 = 0.27
r^2 = 0.01
r^2 = 0.47
r^2 = 0.16
r^2 = 0.01
r^2 = 0.19
r^2 = 0.00
r^2 = 0.43
r^2 = 0.01
r^2 = 0.05

Figure 3.

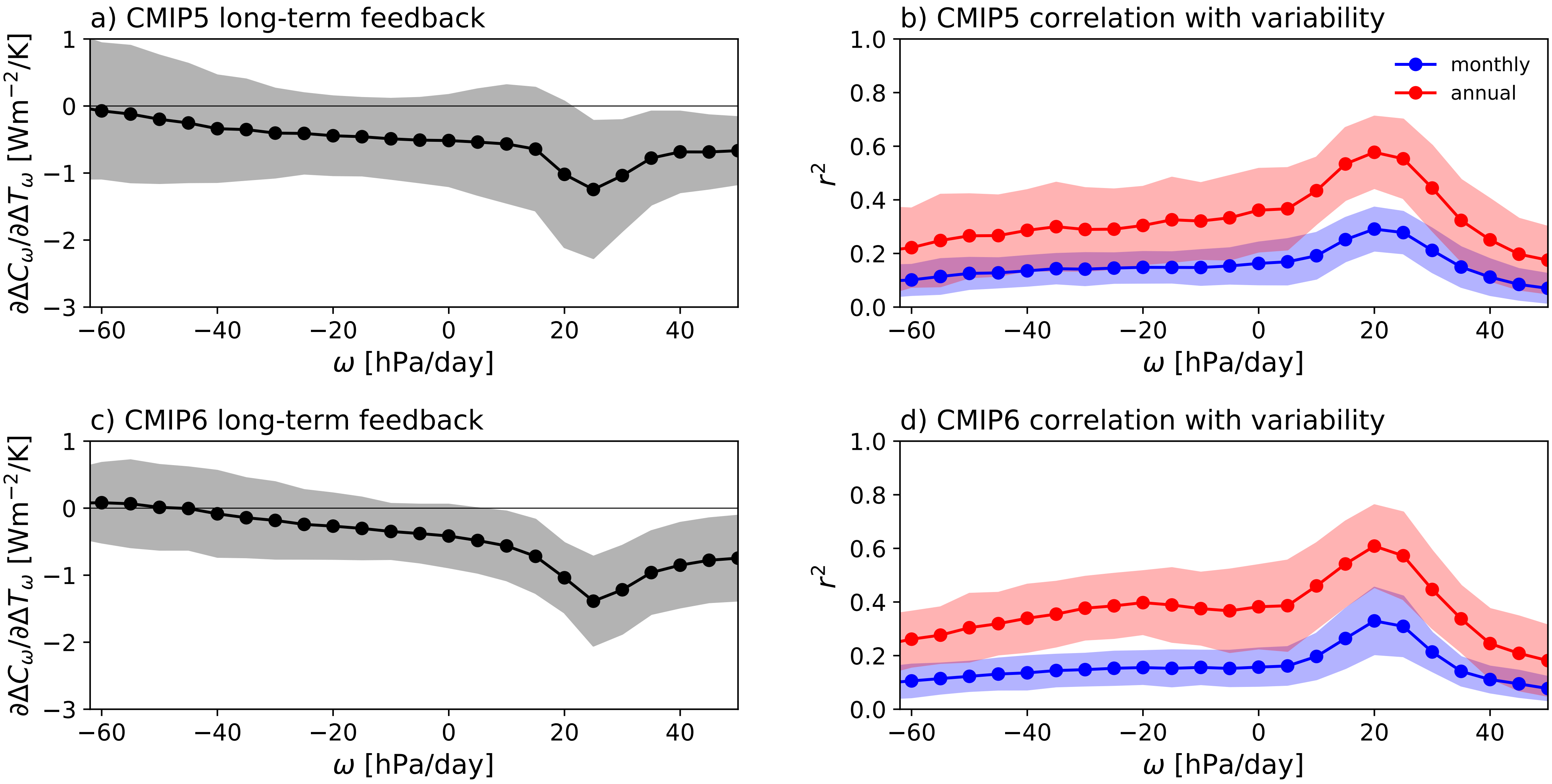

a) CMIP5 long-term feedback
b) CMIP5 correlation with variability
c) CMIP6 long-term feedback
d) CMIP6 correlation with variability
$\partial\Delta C_\omega/\partial\Delta T_\omega$ [Wm^{-2}/K]
r^2
ω [hPa/day]
monthly
annual

Figure 4.

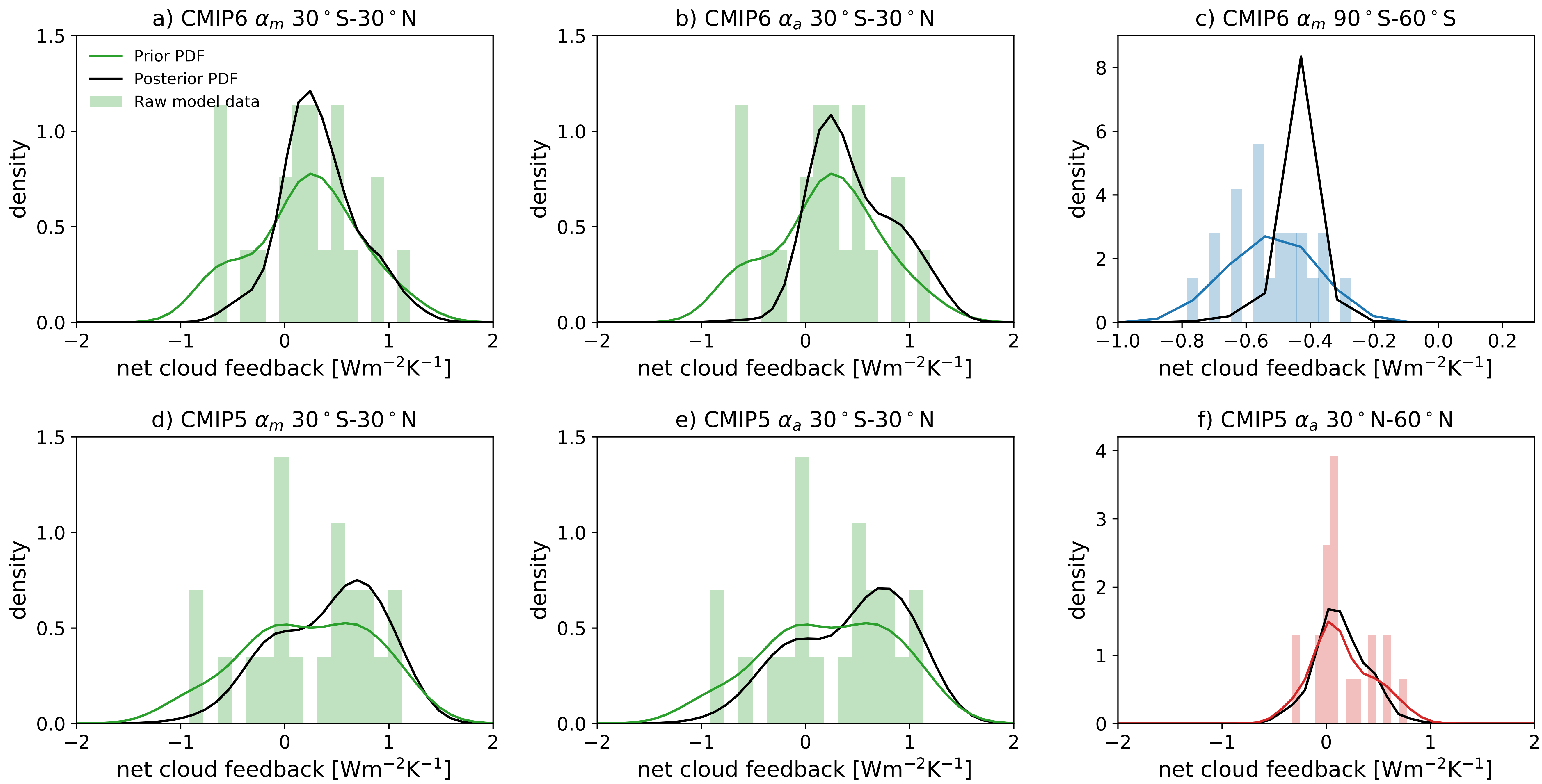

a) CMIP6 α_m 30°S-30°N
b) CMIP6 α_a 30°S-30°N
c) CMIP6 α_m 90°S-60°S
d) CMIP5 α_m 30°S-30°N
e) CMIP5 α_a 30°S-30°N
f) CMIP5 α_a 30°N-60°N
Prior PDF
Posterior PDF
Raw model data
density
net cloud feedback [$Wm^{-2}K^{-1}$]

Supporting Information for "Emergent Constraints on Regional Cloud Feedbacks"

N. J. Lutsko,[1]

Max Popp,[2]

Robert H. Nazarian,[3]

Anna Lea Albright,[2]

Contents of this file

1. Figures S1 to S4
2. Tables S1 and S2

Introduction The supplementary material contains four figures and 2 tables. The first figure shows an example of the the regional "Gregory" plots which are used to estimate the regional cloud feedbacks. The second figure repeats Figure 2 of the main text, but shows the results for the CMIP5 models. Supplemental Figures S3 and S4 repeat Figure 2 of the main text, but show the results when α_m and α_a are calculated using the last 50

Corresponding author: N. J. Lutsko, Scripps Institution of Oceanography, University of California at San Diego, La Jolla, California (nlutsko@ucsd.edu)

[1]Scripps Institution of Oceanography, University of California at San Diego, La Jolla, California.

[2]Laboratoire de Météorologique Dynamique Dynamique, Sorbonne Université, Ecole Normale Supérieure, Ecole Polytechnique, Paris, France.

[3]Department of Physics, Fairfield University, Fairfield, Connecticut.

years of each historical simulation, rather than the last 17 years. Supplemental Figure S3 shows the results for the CMIP6 models and Supplemental Figure S4 shows the results for the CMIP5 models. Table S1 shows the weights used to generate the posterior PDFs for the CMIP5 data and Table S2 shows the weights used to generate the posterior PDFs for the CMIP6 data.

The CMIP5 models used in the analysis are: BNU-ESM, CanESM2, CNRM-CM5, CSIRO-Mk3-6-0, GFDL-CM3, GFDL-ESM2G, GFDL-ESM2M, GISS-E2-H, GISS-E2-R, HadGEM2-ES, INM-CM4, IPSL-CM5A-LR, IPSL-CM5A-MR, IPSL-CM5B-LR, MIROC5, MIROC-ESM, MPI-ESM-LR, MPI-ESM-MR, MPI-ESM-P, MRI-CGCM3, NCAR-CCSM4, NorESM1-M.

The CMIP6 models used in the analysis are: BCC-CSM2-MR, BCC-ESM1, CanESM5, CNRM-CM6-1, CNRM-ESM2-1, FGOALS-f3-L, GFDL-CM4, GFDL-ESM4, GISS-E2-1-G, GISS-E2-1-H,HadGEM3-GC31-LL,INM-CM4-8, IPSL-CM6A-LR, MIROC6, MIROC-ES2L, MPI-ESM1.2-HR,MRI-ESM2-0, NCAR-CESM2, NCAR-CESM2-WACCM, NorESM2-LM, UKESM1-0-102LL. Note that the required data for the ω_{500} binning in Figure 3 of the main text were not available for the following models at the time of the analysis (January 2021): UKESM1-0-LL, MIROC-ES2L, INM-CM4-8, NorESM2-LM, MPI-ESM1-2-HR, MIROC6 and FGOALS-f3-L.

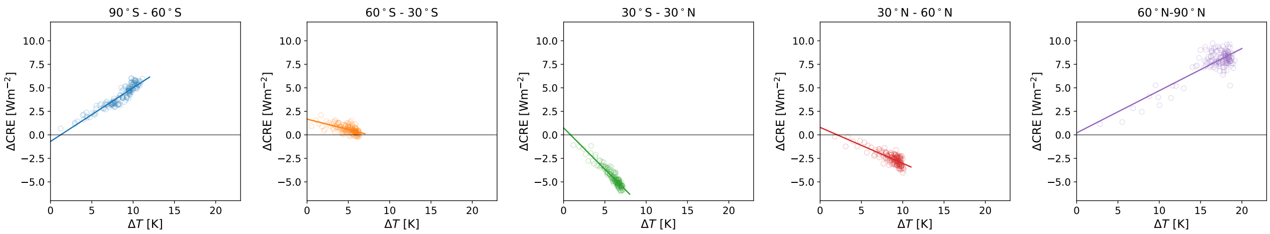

Figure S1. Example of regional "Gregory" CRE plots for the CanESM5 model. The solid lines show linear least-squares regressions to the annual-mean data shown by the open circles.

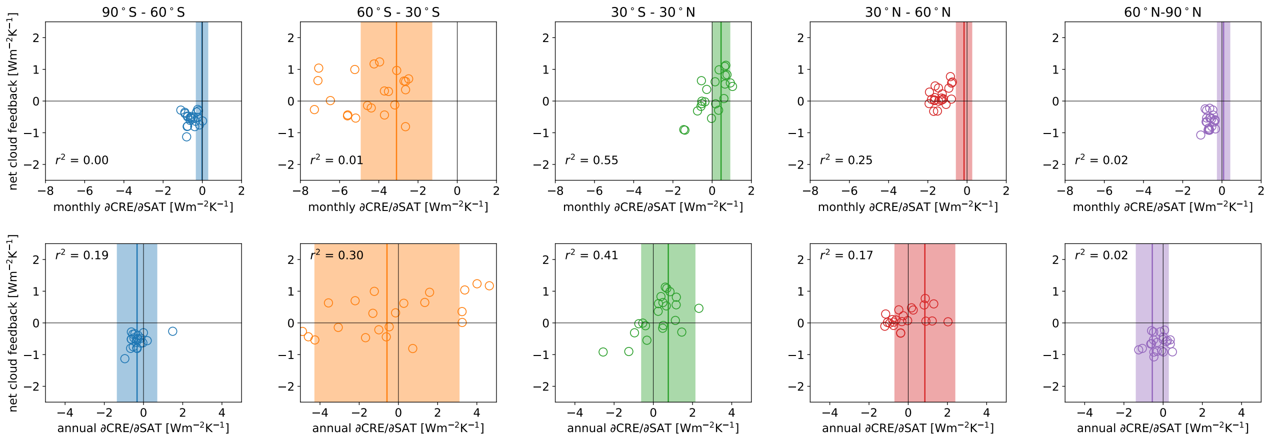

Figure S2. Values of monthly and annual linear regressions of CRE on surface temperatures in the five geographic regions plotted versus the net cloud feedback in each region for 23 CMIP5 models. The regression coefficients are calculated using the last 17 years of the historical simulations. The shaded regions show 5-95% confidence intervals for estimates of the linear regressions from CERES-EBAF data, with the solid lines showing the mean of the observational regression estimates.

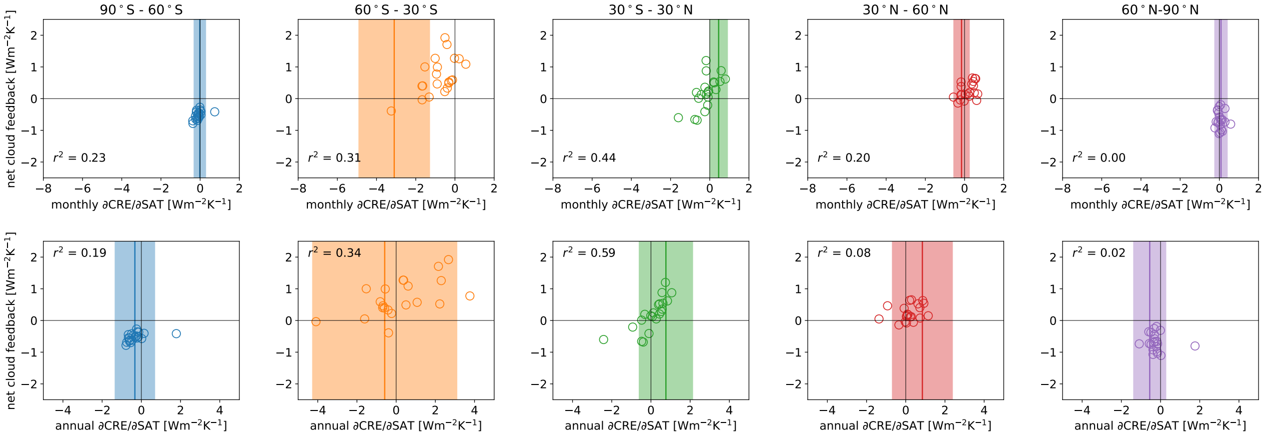

Figure S3. Same as Figure 2 in the main text, but the regression coefficients are calculated using the last 50 years of data in the historical simulations.

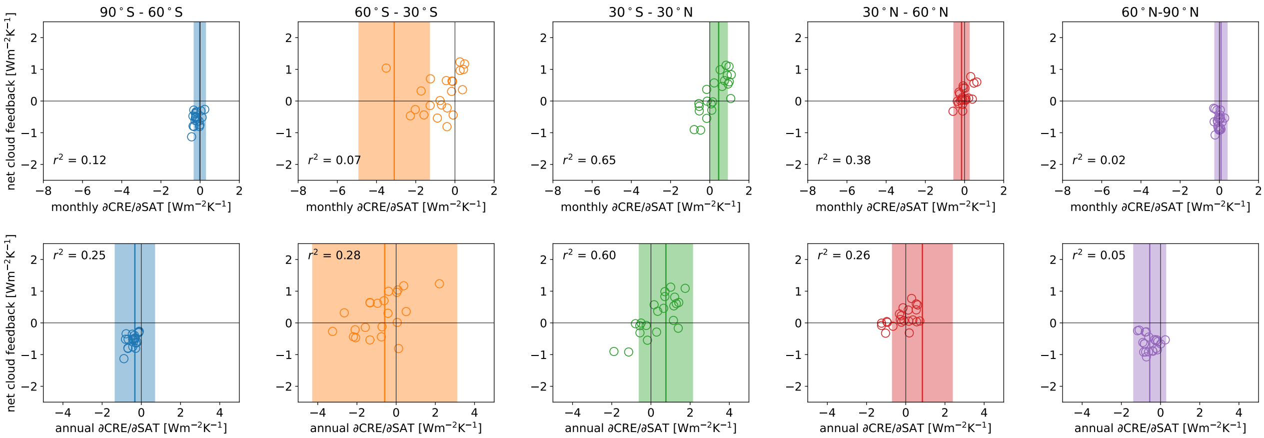

Figure S4. Same as Supplementary Figure S2, but the regression coefficients are calculated using the last 50 years of data in the historical simulations.

Table S1. Weights (in %) used to generate the posterior PDFs for the CMIP5 models. Weights are given for each 17-year segment, and the final posterior PDFs are obtained by averaging the three posterior PDFs obtained from each 17-year segment.

Model	α_m 30°S-30°N	α_a 30°S-30°N	α_m 30°-60°N
BNU-ESM	0.0/9.7/0.7	3.0/7.4/3.4	0.0/0.0/0.0
CanESM2	0.0/0.0/8.3	4.6/0.5/8.5	16.8/3.8/0.0
CNRM-CM5	0.0/0.0/0.0	0.3/0.1/0.0	14.0/3.8/0.0
CSIRO-Mk3-6-0	3.7/11.6/3.8	10.3/6.6/8.9	0.0/0.0/12.8
GFDL-CM3	19.4/0.3/12.1	9.1/7.2/7.5	8.2/0.1/1.4
GFDL-ESM2G	0.0/0.0/0.0	1.0/0.2/0.7	13.1/5.1/0.0
GFDL-ESM2M	0.0/16.6/0.0	0.1/7.2/0.5	4.7/0.0/21.7
GISS-ESM-H	0.0/0.0/0.0	0.0/0.0/0.0	0.1/0.0/0.1
GISS-ESM-R	0.0/2.4/0.0	0.0/2.7/0.0	12.5/0.0/0.0
HADGEM2-ES	15.0/13.7/10.7	11.5/7.0/6.6	0.0/0.7/2.7
INMCM4	7.1/0.2/11.3	6.6/4.9/7.6	16.1/33.3/21.0
IPSL-CM5A-LR	0.0/0.0/8.5	1.6/0.0/7.6	0.0/0.0/0.0
IPSL-CM5A-MR	6.4/0.0/10.2	11.6/3.6/8.5	0.0/0.0/0.0
IPSL-CM5B-LR	18.3/0.1/9.1	4.7/4.8/4.8	5.6/0.0/0.0
MIROC5	9.5/1.3/0.0	6.2/3.1/5.5	0.0/0.0/9.4
MIROC-ESM	1.7/11.4/1.6	9.4/7.3/7.2	0.0/0.0/0.0
MPI-ESM-LR	0.0/18.0/0.0	0.1/8.1/0.1	0.0/7.6/0.0
MPI-ESM-MR	0.1/3.0/8.3	3.2/7.4/3.7	8.5/0.0/0.0
MPI-ESM-P	0.0/2.7/0.0	3.8/7.7/1.5	0.0/0.5/0.5
MRI-CGCM3	18.6/0.2/3.0	10.9/5.2/7.6	0.0/0.0/0.2
NCAR-CCSM4	0.0/2.0/12.5	0.8/3.4/8.2	0.0/9.4/23.1
NorESM1-M	0.0/6.8/00	1.3/5.7/1.1	0.0/35.4/7.0

Table S2. Weights (in %) used to generate the posterior PDFs for the CMIP6 models. Weights are given for each 17-year segment, and the final posterior PDFs are obtained by averaging the three posterior PDFs obtained from each 17-year segment.

Model	α_m 30°S-30°N	α_a 30°S-30°N	α_m 60°-90°S
BCC-CSM2-MR	0.1/12.5/0.5	6.8/4.7/8.0	0.0/0.7/2.2
BCC-ESM1	0.0/4.3/0.1	6.5/8.7/9.7	0.0/4.0/0.2
CanESM5	12.2/12.9/0.6	10.7/9.5/10.0	0.0/1.2/0.6
CNRM-CM6-1	0.1/9.6/12.4	3.8/3.7/0.7	98.0/60.9/8.5
CNRM-ESM2-1	15.9/7.6/4.3	0.8/4.7/3.7	1.7/2.1/0.0
FGOALS-f3-L	2.4/0.0/0.0	0.2/0.0/0.1	0.0/0.0/0.0
GFDL-CM4	0.9/5.9/12.7	7.6/8.8/9.3	0.0/0.0/0.0
GFDL-ESM4	3.5/12.9/1.8	5.2/1.9/8.9	0.0/0.0/0.0
GISS-E2-1-G	0.0/0.0/0.0	0.0/0.0/0.0	0.0/0.0/0.0
GISS-E2-1-H	0.0/0.0/0.0	0.0/0.1/0.0	0.0/0.0/0.0
HadGEM3-GC31-LL	1.3/0.7/3.9	3.1/3.8/8.4	0.2/2.6/1.4
INM-CM4-8	0.0/0.0/0.0	0.0/0.0/1.6	0.0/0.0/3.9
IPSL-CM6A-LR	13.1/8.9/11.5	9.7/9.9/4.3	0.0/27.0/0.0
MIROC6	17.5/5.1/14.4	4.8/7.1/1.0	0.0/0.0/0.0
MIROC-ES2L	3.1/0.0/11.1	0.0/0.0/0.0	0.0/0.0/0.0
MPI-ESM1.2-HR	1.9/0.0/10.2	2.8/0.3/9.4	0.0/0.0/0.0
MRI-ESM2-0	10/3.5/2.2	6.9/1.7/1.3	0.0/0.1/0.9
NCAR-CESM2	5.5/1.9/4.3	10.3/7.8/8.6	0.0/0.1/0.0
NCAR-CESM2-WACCM	4.9/2.7/2.0	9.9/8.6/9.0	0.0/0.2/0.0
NorESM2-LM	7.7/8.2/8.1	8.3/9.1/4.5	0.0/0.6/82.2
UKESM1-0-102LL	0.0/2.3/0.0	2.7/9.6/1.6	0.0/0.1/0.0